

## Oceanographic observations at the shelf break of the Amundsen Sea, Antarctica

Dziga P. Walker,<sup>1</sup> Adrian Jenkins,<sup>1</sup> Karen M. Assmann,<sup>1</sup> Deborah R. Shoosmith,<sup>1</sup> and Mark A. Brandon<sup>2</sup>

Received 28 November 2012; revised 27 March 2013; accepted 22 April 2013; published 13 June 2013.

[1] The glaciers draining into the Amundsen Sea Embayment are rapidly losing mass, making a significant contribution to current sea level rise. Studies of Pine Island Glacier (PIG) in this region indicate that the mass loss is associated with rapid melting of its floating ice shelf driven by warm Circumpolar Deep Water (CDW) that is able to penetrate all the way to its grounding line, and that recent intensification of the mass loss is associated with higher melt rates and stronger subice-shelf circulation. CDW is sourced from within the Antarctic Circumpolar Current (ACC) situated well north of the glacial ice fronts. To be able to access the Amundsen Sea glaciers, CDW must first cross the continental shelf break where the deep ocean meets the shallower waters of the continental shelf. Here, we present data that shows how CDW moves along the continental slope and across the shelf break into the Amundsen Sea. On-shelf flow of CDW is enhanced where a subsea trough bisects the shelf edge. A previously unreported undercurrent is observed flowing eastward along the shelf edge and when this current encounters the trough mouth it circulates southward into the trough and toward the glaciers. Upwelling associated with this trough circulation appears to allow Lower CDW onto the shelf that would otherwise be blocked by the topography. These observations concur with the results of a theoretical modeling study of circulation in a similar topographic setting and also with the results of a regional ocean/ice modeling study of the Amundsen Sea specifically.

**Citation:** Walker, D. P., A. Jenkins, K. M. Assmann, D. R. Shoosmith, and M. A. Brandon (2013), Oceanographic observations at the shelf break of the Amundsen Sea, Antarctica, *J. Geophys. Res. Oceans*, 118, 2906–2918, doi:10.1002/jgrc.20212.

### 1. Introduction

[2] The glaciers that drain into the Amundsen Sea Embayment are among the World's fastest dischargers of ice into the ocean [Rignot *et al.*, 2008]. These glaciers originate from one of the largest drainage basins of the West Antarctic Ice Sheet (WAIS), complete collapse of which could cause a 3.3 m rise in global eustatic sea level [Bamber *et al.*, 2009]. A catalog of remotely sensed data from the last 30 years reveals a pattern of change that extends from the floating ice tongues [Rignot, 2002; Shepherd *et al.*, 2004], up through the fast moving glacial ice streams [Rignot, 2008; Joughin *et al.*, 2010] all the way into the deep interior of the WAIS [Wingham *et al.*, 1998; Shepherd *et al.*, 2001]. These observations have prompted questions regarding the long-term stability of the WAIS and the rate at which further deglaciation may occur.

[3] One of the key factors determining the increasing mass loss to the sea is ocean-driven melting caused by the presence of warm CDW that dominates the Amundsen Sea continental shelf beneath the colder surface layers and circulates beneath the floating ice tongues [Jacobs *et al.*, 1996]. A sporadic observation database, gathered over the past two decades, indicates that while always present, the core properties and thickness of the layer of CDW on the shelf does vary [Jacobs *et al.*, 2011]. Results of a regional ocean/ice modeling study suggested that variability is associated with variability in the inflow of CDW to the shelf that is itself influenced by local wind forcing [Thoma *et al.*, 2008]. Ding *et al.* [2011] demonstrated a link between atmospheric circulation over the Amundsen Sea and central tropical Pacific sea surface temperature, raising the possibility of a causal link between far-field climate forcing and thinning and acceleration of WAIS outlet glaciers [Steig *et al.*, 2012]. In 2009, autonomous underwater vehicle observations from beneath the floating tongue of PIG [Jenkins *et al.*, 2010] revealed large volumes of CDW within the cavity, but also a seafloor ridge that partially shielded the inner cavity from the warmest waters. That discovery highlighted the potential role of local seabed geometry in dictating recent dynamical changes in both ice and ocean, with the possibility that the ongoing ice sheet retreat is a self-sustaining response to an earlier extreme of climate forcing or simply an accelerated phase of long-term

<sup>1</sup>British Antarctic Survey, Natural Environment Research Council, Cambridge, UK.

<sup>2</sup>Centre for Earth, Planetary, Space and Astronomical Research, Open University, Milton Keynes, UK.

Corresponding author: D. P. Walker, British Antarctic Survey, Natural Environment Research Council, High Cross, Madingley Road, Cambridge CB3 0ET, UK. (dziga.walker@gmail.com)

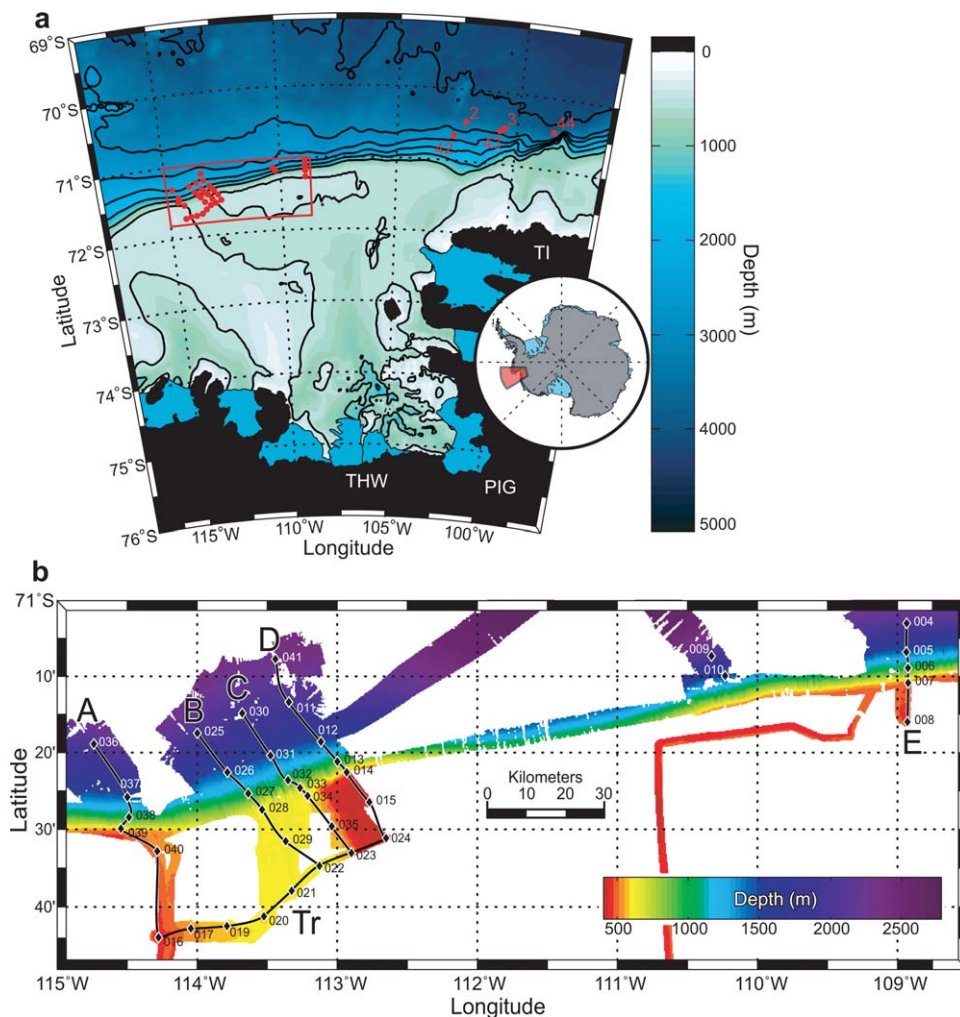


**Figure 1.** (a) The Amundsen Sea Embayment with locations of CTD stations shown as red dots. The red box bounds the area shown in Figure 1b. Ice shelves are shown as filled blue areas and black areas represent grounded ice and rock. Black contours represent the 500, 1000, 1500, 2000, 2500, 3000 and 4000 m isobaths. TI, PIG, and THW are Thurston Island, Pine Island Glacier, and Thwaites Glacier, respectively. Bathymetry data arranged by *Timmerman et al.* [2010]. (b) Acoustic multibeam-derived bathymetry showing the topographic features of the shelf edge and the locations of CTD stations (numbered black diamonds). The across-shelf sections (labeled A–E) and trough section (Tr) are shown in black lines.

deglaciation [*Schoof*, 2007]. An analysis of oceanographic data collected at the PIG ice front in 1994 and 2009 showed a 50% increase in ice shelf melting and an 80% increase in the strength of the subice ocean circulation despite modest changes in CDW properties [*Jacobs et al.*, 2011], and hinted at a key role for seabed and/or evolving ice geometry in at least modulating the response to far-field ocean forcing. Untangling the complex interplay between local geometrical control on the access of ocean heat to the grounding line and climate forcing of broader-scale ocean variability on the Amundsen Sea shelf is perhaps the single most critical step needed to address the question of how the glaciers will evolve into the future. As a contribution to that broad aim, this study focuses on the critical region at the shelf edge, where CDW is delivered from the deep ocean to the Amundsen Sea continental shelf. Variability of that delivery was highlighted by *Thoma et al.* [2008] as

a key factor in the transmission of far-field climate forcing into the ocean properties experienced by the ice shelves.

[4] Far-field CDW is characterized by a subsurface temperature maximum between 1.6 and 2.0°C and salinities greater than 34.6 psu. It is often subdivided into Upper CDW (UCDW) and Lower CDW (LCDW) with UCDW characterized by a temperature maximum and dissolved oxygen minimum, whereas the fractionally cooler LCDW below is associated with higher salinities (>34.7 psu). In a circumpolar study of the continental margin, *Whitworth et al.* [1998] used neutral density [*Jacket and McDougall*, 1997] to separate the boundaries between overlaying Antarctic Surface Water (AASW), the cold, saline shelf waters (SW), and Antarctic Bottom Water (AABW) found below. In the south east Pacific, CDW has neutral densities between 28.00 and 28.27 kg m<sup>-3</sup> with AASW less than 28.00 kg m<sup>-3</sup> and AABW/SW greater than 28.27 kg m<sup>-3</sup>

[Whitworth *et al.*, 1998]. CDW is the world's most voluminous water mass and fills most of the water column of the entire Southern Ocean, flowing perpetually eastward within the ACC. The ACC flows close to the continental margin of the south east Pacific sector of Antarctica, thus bringing CDW close to the transition zone between the deep oceanic waters and the shallower continental shelf.

[5] Here, we report data gathered during a 2003 survey of the region around 113–114°W where a northeast/southwest trending seabed trough cuts the shelf break. The survey comprised five synoptic across-shelf transects, of which four were located around the mouth of the trough and the fifth about 150 km further to the east. An additional along-shelf (zonal) conductivity, temperature, and depth (CTD) section was surveyed across the trough approximately 25 km inshore of the shelf edge. From the bathymetry data available, the trough appears to be one of two such shelf-edge features that link to the main north/south trough on the eastern Amundsen Sea continental shelf (Figure 1). On the inner shelf, the eastern trough attains its maximum depth of around 1600 m to the north of Thwaites Glacier Tongue, and is believed to be the main route by which CDW is channeled toward the ice fronts [Walker *et al.*, 2007, Thoma *et al.*, 2008, Jacobs *et al.*, 2011; Schodlok *et al.*, 2012].

[6] In this paper, we discuss the water mass structure across the continental margin, particularly the along-shelf current structure and its potential to permit CDW to flood the shelf. The following section describes the instruments and the methodology applied to calculate absolute geostrophic velocities. The results section presents the major oceanographic features and describes the temperature, salinity, and velocity sections obtained from the data. Section four discusses the implications of our findings with particular reference to a previously unreported undercurrent and how it compares with other observational and theoretical studies of similar features followed by a summary of the main conclusions.

## 2. Data and Methods

### 2.1. Hydrographic Data

[7] All CTD data were gathered in March 2003 aboard the *RRS James Clark Ross* (cruise JR84) where a total of 44 CTD stations were collected. The CTD system used was a Sea-Bird 911 Plus with dual temperature and conductivity sensors, an altimeter, dual-SBE 43 oxygen sensors, a high-precision SBE 35 reference temperature sensor, and a 12 bottle carousel water sampler. The sensors were all calibrated 6 months prior to the cruise. Additionally, a Guildline Autosol salinometer was used in a temperature controlled laboratory on board to measure the conductivity of discrete water samples and these data were used to derive precise calibration offsets for the primary conductivity sensor.

[8] The geographical context of this work is shown in Figure 1. The canyon is clearly visible where it cuts the shelf edge between 113°W and 114°W. All of the across-shelf sections (A–E) started in 2000 m water depth and subsequent stations were occupied at 500 m depth intervals up the continental slope and onto the shelf. Additional CTD stations were occupied to the north of Thurston Island in

water depths of between 3000 and 4000 m at the base of the continental rise, at the eastern edge of the Amundsen Sea. Although these stations do not form part of synoptic sections, they do extend our data set zonally along the continental margin providing a longitudinal perspective of the Amundsen Sea.

### 2.2. Hull-Mounted ADCP Data

[9] The *RRS James Clark Ross* was fitted with an RD Instruments 153.6 kHz ship-mounted acoustic Doppler current profiler (SADCP). Absolute velocities were calculated using heading data acquired with a Sperry Mk37 gyrocompass that were corrected using additional satellite-derived heading data measured by an Ashtec ADU-2 Global Positioning System (GPS) [King and Cooper, 1994]. Positional data were acquired using a Trimble 4000 GPS receiver operating in differential mode (Differential GPS) using GPS range corrections sent via Inmarsat B that were transmitted from Rothera Research Station, situated on Adelaide Island west of the Antarctic Peninsula. Full details of all data processing may be found in the JR84 Cruise Report (unpublished report, 2003) available from the British Oceanographic Data Centre (<http://www.bodc.co.uk/>). We eliminated all data where the percentage of good pings received were less than 75%, resulting in near continuous current data for the upper 350 m of the water column. Based on the standard error of the SADCP data and the precision of the navigational systems, we estimate the error of our velocity data to be within  $\pm 3 \text{ cm s}^{-1}$ .

### 2.3. SADCP Detiding

[10] SADCP data are used in this work to provide a reference for the relative geostrophic velocities derived from CTD data to derive absolute geostrophic velocity profiles. Prior to doing this, tidal currents need to be removed from the SADCP, leaving the lower frequency (subtidal) features that we are interested in. Two methods for deriving tidal currents were applied; harmonic analysis of the SADCP data and interpolation of output from the Circumpolar Antarctic Tidal Simulation 2008 model (CATS2008b) [Padman *et al.*, 2002].

[11] The harmonic analysis technique uses a traditional least squares approach to fit the four main tidal components to the SADCP record using spatially varying coefficients [Allen, 1995]. The technique has been applied successfully to SADCP data from the Iceland-Faeroe Gap in the North Atlantic, where results compared favorably with those from a tidal model [Allen, 1995], whereas an analogous technique has been successfully applied in the tidally dominated East China Sea and on the Amazon shelf, where subtidal and tidal currents are of similar magnitude [Candela *et al.*, 1992]. In our study, a continuous 22 day record of SADCP data was used for the detiding procedure, sufficient to resolve the four primary tidal constituents. The 22 day record starts at the north end of the Antarctic Peninsula, and covers the entire transit to the Amundsen Sea, the work period there, and the transit back to Adelaide Island, west of the Peninsula during March 2003.

[12] Additionally, predicted barotropic tidal currents along the same length of cruise track were extracted from CATS2008b, which is forced at its open boundary by tidal heights from the global inverse model TPX07.1,

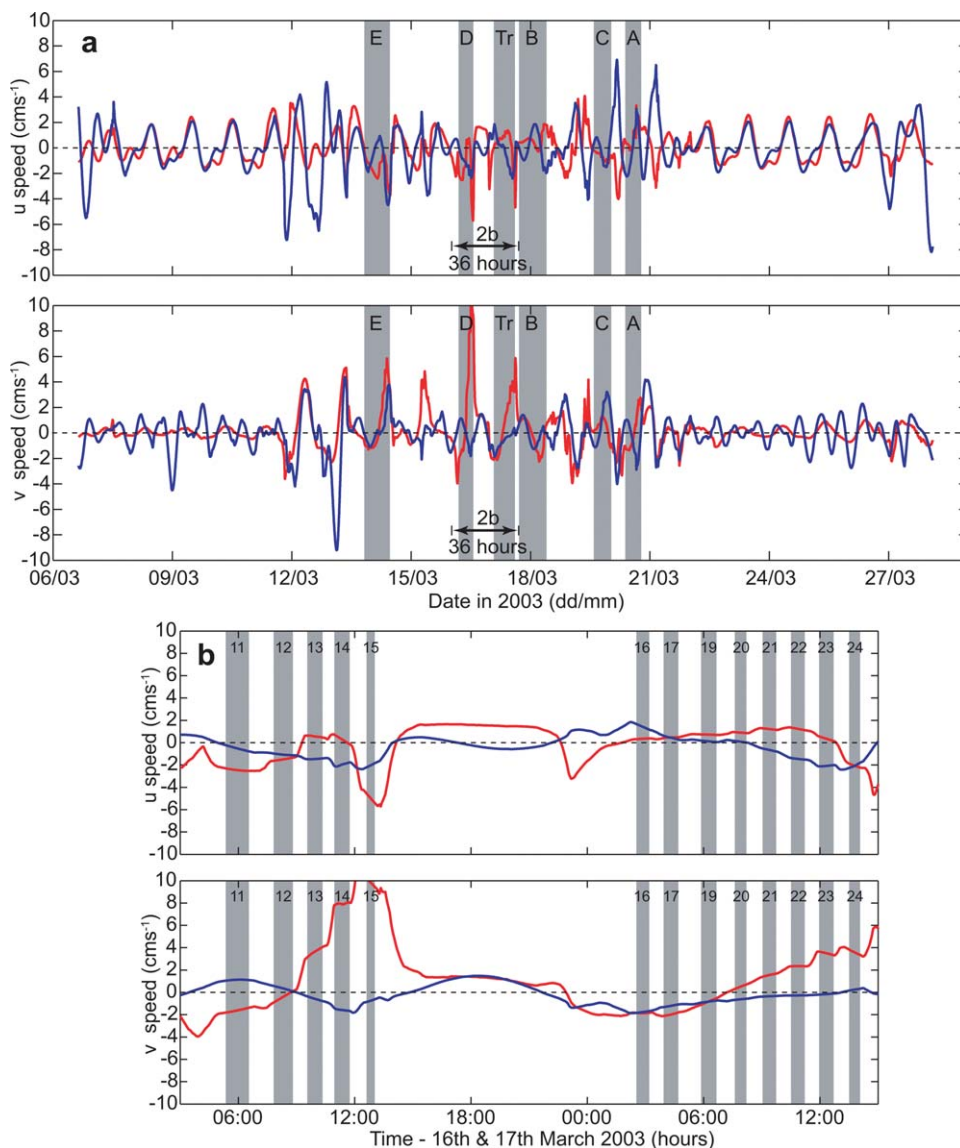


**Figure 2.** (a) Comparison of SADCPC empirically derived tidal currents (blue lines) and CATS2008b model predicted currents (red lines) for a 22 day long section of ship's tracks. (top) East-west tidal current speed ( $u$  positive eastward). (bottom) North-south tidal current speed ( $v$  positive northward). Time periods where the ship was undertaking specific CTD sections are grayed out and labeled. (b) The 36 h subsection of the time period arrowed in Figure 2a which includes sections D and Tr. Gray regions represent the times the ship was on-station collecting CTD data (numbered).

incorporates the best available bathymetry and simulates the 10 primary tidal constituents on a 4 km grid. Where available, measured Antarctic tidal height data have been assimilated into the model, although no such data exist for the Amundsen Sea region.

[13] Due to the lack of any permanent tidal station in the region, there are no suitable reference data with which to validate either method with any certainty. However, the use of two independently derived tides gives an overall indication of the significance of the tide when considering the main (subtidal) results. Figure 2a shows the east-west ( $u$ ) and north-south ( $v$ ) tidal currents along the ship's track obtained by each method for the complete 22 day record. It also highlights the specific times when detided SADCPC

data have been extracted to reference the relative geostrophic velocities for each CTD section. Overall, the two predicted tides are of a similar magnitude with only a few discrete periods of significant disagreement. Perhaps unsurprisingly the best agreement occurs for the periods from the 8th to 12th March and from the 22nd to 26th March, the two periods when the ship was steaming over the deep waters of the southeast Pacific en route to and returning from the Amundsen Sea. At those times, the phase and amplitude of the east-west currents show particularly good agreement, although discrepancies remain between the north and south currents.

[14] The individual components of the tidal currents derived by either method have amplitudes that are typically

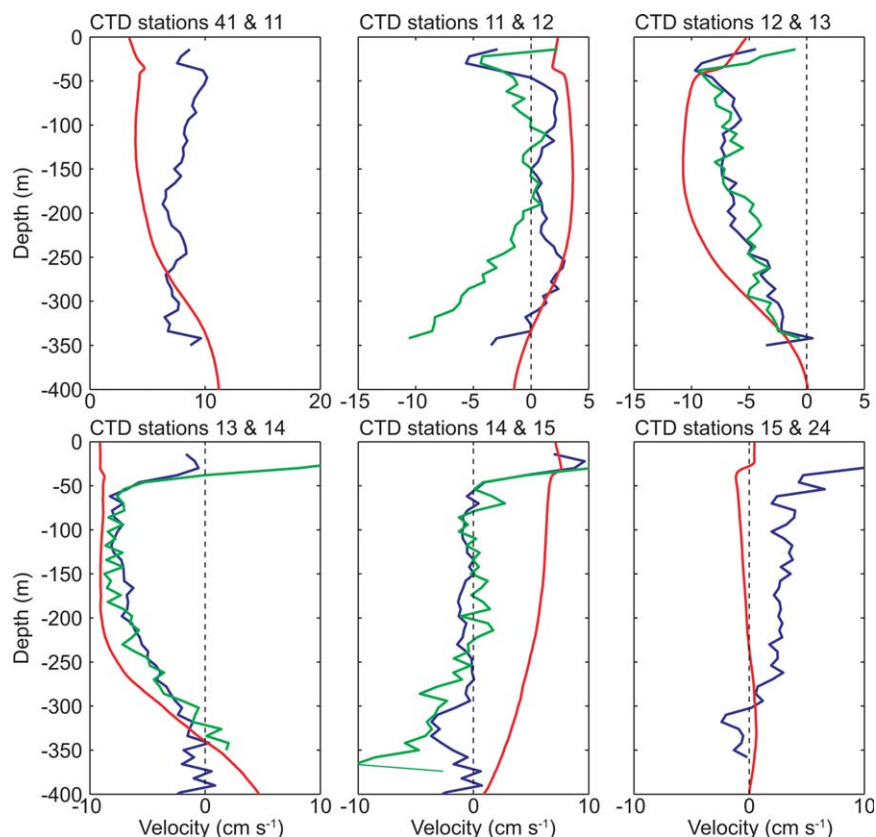


**Figure 3.** Comparison of velocity shears for the upper 400 m calculated using CTD data and SADC data for each CTD station pair that make up Transect D. Red curves are the geostrophic shears relative to zero at the deepest common level. Blue lines are the SADC velocities obtained using on-station pair averaging and the green lines are from the SADC underway data between each station pair. Positive values are eastward flow.

around  $3 \text{ cm s}^{-1}$  or less. However, there are brief periods when each method predicts current “spikes” well in excess of  $5 \text{ cm s}^{-1}$  and more often than not these spikes are not coincident in the two records. So despite generally small differences between the records, with a mean absolute difference in  $u$  and  $v$  of only  $1.33$  and  $1.13 \text{ cm s}^{-1}$ , respectively, maximum differences of  $10.57$  and  $12.98 \text{ cm s}^{-1}$ , respectively, occur at the times of the most extreme current spikes.

[15] It can be seen in Figure 2a that some of the largest amplitudes and absolute differences occur during CTD sections, particularly those on sections D and Tr. This is shown in detail in Figure 2b, which covers the 36 h period during which both of those sections were measured. In both cases, the empirically derived tide is weaker with amplitudes of less than  $2 \text{ cm s}^{-1}$ , whereas the CATS2008b currents are more variable, especially for the north-south component. Although the largest current amplitudes and absolute differences between the two tides are coincident with specific CTD sections, the choice of tide ultimately made little difference to the main circulation features reported in this work. Even when the tidal predictions disagreed the most, the inferred subtidal circulation patterns remained present regardless of which prediction was used to detide the SADC data, giving us confidence that the derived velocity sections are representative of the subtidal current structure.

#### 2.4. Geostrophic Velocity Referencing

[16] In addition to removing the tide, suitable subsections of SADC data must be chosen to reference the CTD-derived relative geostrophic currents. The detided SADC data were subdivided into periods when the vessel was conducting CTD’s while holding position, and periods when the ship was steaming between stations. Records from the transition periods between holding position and maintaining a steady course to the next station were carefully screened to remove any data that had been contaminated by the inability of the navigational instruments to resolve the vessel’s acceleration. Underway data between stations were averaged and the component perpendicular to the section line calculated to give a mean cross-track current profile between each CTD pair. Additionally, the mean “on-station” SADC profiles for each CTD were pair averaged, the resulting component perpendicular to the section line giving an alternative estimate of the mean cross-track current between the two CTDs. In some locations, no representative underway data existed so only the on-station SADC pair-averaged data could be used.

[17] The detided SADC data from the topmost 350 m of the water column provided a layer of known absolute velocity that could then be used as a reference to adjust the relative geostrophic velocity profiles. Following careful examination of all of the unreferenced geostrophic and

SADCP profiles together, the most suitable depth range for calculating the offset used to adjust the relative geostrophic currents was found to be 102–302 m. That depth range excluded any possible transient ageostrophic flow in the surface wind-driven layer as well as any noise at the deeper end of the SADCP profiles, which was present in some cases. Figure 3 shows a comparison of velocity shears (relative geostrophic, SADCP on-station, and underway profiles) for transect D. In general, the shape of the SADCP profiles derived from both underway and on-station pair-averaged data agree reasonably with the geostrophic shears, implying that the SADCP data below the wind-driven layer is representative of the geostrophic flow structure. Overall, it appears that the underway SADCP data give a marginally better representation of the geostrophic shear (between stations 11 and 12, in Figure 3 for example), perhaps not surprising given that those data are a direct measure of the currents of interest.

[18] Offsets were obtained for each CTD pair and applied to the unreferenced geostrophic shears to calculate the absolute geostrophic velocity profiles used in this study. In total, we have two independently predicted tides and two measures of absolute velocity over the reference layer between 102 and 302 m. Using all possible combinations of these, we are better able to discern the overall success of the referencing technique as well as test the robustness of features that may or may not result from tidal or ageostrophically contaminated SADCP data. Figure 4 shows the calculated velocities for section D derived using both detided data sets with both underway and onstation SADCP data. As noted above, section D contains the most extreme spike in the predicted tidal currents so the comparison represents a worst case scenario for the impact of the unknown tide on the final derived velocity data. The effect of the strong CATS2008b tide can be seen in the southern half of the section where there is at most a  $6 \text{ cm s}^{-1}$  difference caused by the choice of tidal prediction. Although the difference in north-south tidal currents exceeded  $12 \text{ cm s}^{-1}$  over this part of the section, the orientation of the section is such that differences in the current component perpendicular to the section are somewhat smaller. The differences resulting from the use of underway versus on-station SADCP data are barely noticeable, except between CTDs 11 and 12 where the westward flow is weaker by approximately  $3 \text{ cm s}^{-1}$  in the on-station calculations.

[19] Similar comparisons were made for all of the sections and the findings were very similar throughout. For the trough section, the choice between on-station and underway SADCP data had a slightly larger impact, with the largest difference being a  $5 \text{ cm s}^{-1}$  change in an off-shelf flowing core between CTDs 19 and 20. However, the general circulation patterns remained the same across the entire trough section regardless of whether on-station or underway data were used. Although the underway averaged SADCP data are a slightly better match for the geostrophic profiles, the method cannot be applied to the southernmost station pair of each across-shelf transect (and the northernmost pair of section D), an example of which can be seen in the first and last panel in Figure 3 where only on-station SADCP data exist. For the purpose of consistency throughout, the on-station data were used to reference all of the geostrophic shear profiles. As with all sections, the choices

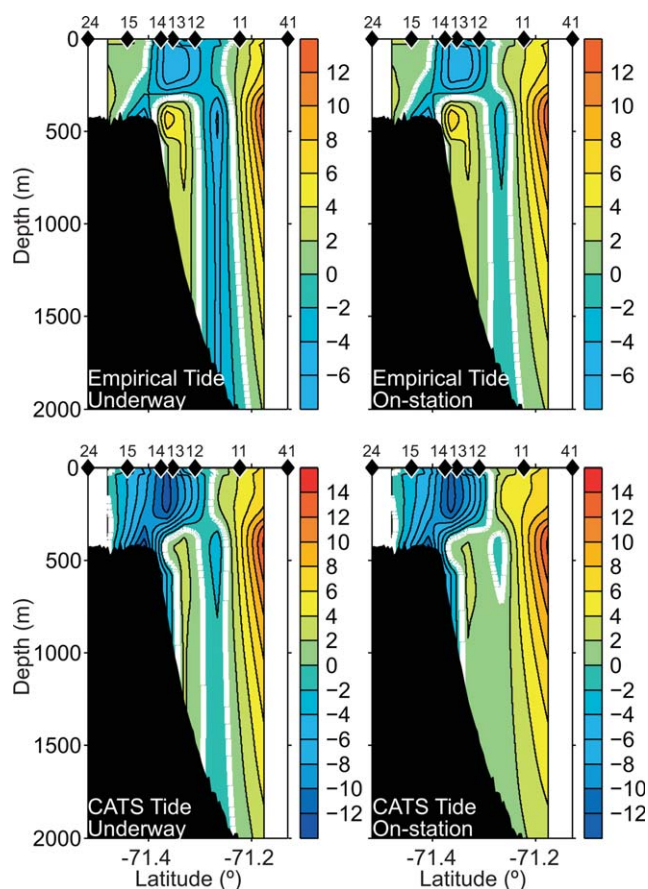


**Figure 4.** Meridional velocity sections for transect D derived using different methods. Color contours are velocity in  $\text{cm s}^{-1}$ . The top figures were both detided using the empirically estimated tide and the bottom figures were detided using CATS2008b tidal predictions. The left figures were referenced using underway SADCP and the right figures used on-station pair-averaged SADCP data.

of detiding and referencing techniques were found to have no significant impact on the overall flow patterns discussed below, giving confidence that the derived velocity sections are representative of the subtidal structure.

### 3. Results

#### 3.1. Water Masses and Hydrographic Sections

[20] Figure 5 shows a potential temperature—salinity ( $\theta$ - $S$ ) plot of all of the Amundsen Sea CTD data collected on the JR84 Cruise, while Figure 6 shows potential temperature, salinity, and velocity sections for the five across-shelf transects (sections A–E). The velocity sections are discussed in section 3.2. The only distinct water masses in the entire data set are CDW (comprising subdivisions of UCDW, LCDW, and modified CDW) and AASW (including Winter Water, WW). We use *Whitworth et al.*'s [1998] neutral density definition ( $\sigma^{\theta} = 28.00 \text{ kg m}^{-3}$ ) to classify the boundary between the regional variety of off-shelf (source) CDW and the overlying surface water masses.

[21] At the sea surface, we find AASW showing typical summertime spatial  $\theta$ - $S$  variability caused by exchanges at the air-sea interface and freshening due to melting sea ice.

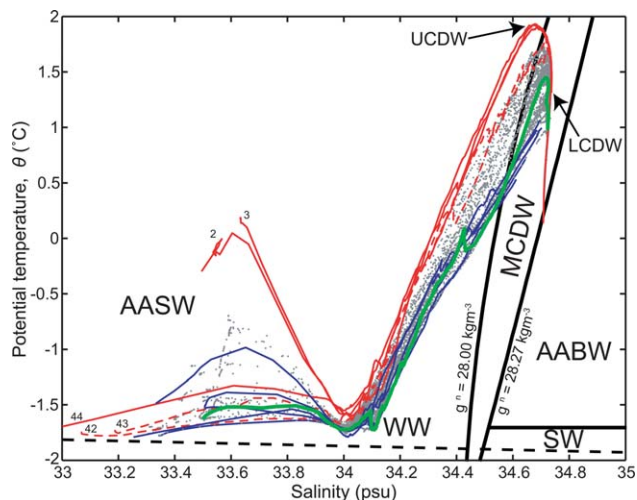


**Figure 5.** Potential temperature—salinity ( $\theta$ - $S$ ) plot of the JR84 Amundsen Sea CTD data (stations 2–44). The water mass boundaries in black lines are those described in section 1. The black dashed line is the freezing point of seawater at the surface. Red lines indicate the five deep CTD stations (CTD stations 2, 3, 42, 43, and 44 labeled) that were taken at the base of the continental rise north of Thurston Island in depths between 3000 and 4000 m. The four blue lines are the four shallowest CTD stations located in shelf water with depths less than 480 m (CTD stations 8, 15, 16, 24, not labeled). The green line is CTD station 22 referred to in the text.

Deeper in the water column, the distinct temperature minimum WW layer is found tightly clustered in  $\theta$ - $S$  space with salinities around 34.0 psu and temperatures less than  $-1.5^{\circ}\text{C}$ . Beneath the WW layer is the main thermocline separating the cold surface waters from the CDW beneath. We find no water masses denser than CDW in this data set, such as AABW or saline SW that are commonly found around Antarctica. The densest water mass in the entire data set is LCDW found offshore of the shelf edge at depths of  $\sim 700$  m down to the seafloor.

[22] CTD stations 2, 3, 42, 43, and 44 were recorded in deep water (3000–4000 m) at the base of the continental rise in the eastern Amundsen Sea, north of Thurston Island (Figure 1a). Although some distance east of the main shelf break sections, they provide a valuable regional context for those more westerly observations, revealing hydrographic properties that can be associated with the ACC. The red lines in Figure 5 represent these deep CTD stations, three of which (2, 3, and 44) have a distinctly warmer and shallower subsurface CDW temperature maximum ( $\theta_{\text{max}} = 1.9^{\circ}\text{C}$ ) and a fractionally warmer (by about  $0.3^{\circ}\text{C}$ ) WW core. Such shoaling of the UCDW and consequent warming of the WW is seen throughout the southern limb of the ACC. Orsi *et al.* [1995] identified the subsurface  $\theta_{\text{max}} = 1.8^{\circ}\text{C}$  as being a circumpolar indicator of the southern ACC front (SACCF). By this definition, these three stations were north of the SACCF at the time of measurement, locating the SACCF at the base of the continental rise north of Thurston Island near the 3000 m isobath. Consistent with this interpretation, CTD stations 42 and 43 have the distinctively colder CDW core properties that would be

expected just to the south of the SACCF, with temperature maxima of  $1.77$  and  $1.67^{\circ}\text{C}$ , respectively. CTD station 43 was occupied 2 weeks after CTD station 3, but both were taken at nearly the same location (less than 9 km between them). Their differing properties either indicate that the SACCF passed directly through the 9 km gap, or provide evidence of the SACCF meandering over time, behavior that has been observed elsewhere [Thorpe *et al.*, 2002].

[23] Further to the west, none of the across-shelf transects (sections A–E) have subsurface temperature maxima greater than  $1.8^{\circ}\text{C}$  suggesting that the SACCF in that region is north of the continental slope. However, the sections all commenced at the 2000 m depth contour, inshore of the 3000 m contour where we found the SACCF further to the east near Thurston Island. While departing the Amundsen Sea an additional CTD station (41) was occupied, extending transect D off-shelf by 6 km into approximately 2300 m water depth, where the temperature maximum was  $1.73^{\circ}\text{C}$ . Between CTD stations 11 and 41, shoreward shallowing isopycnals fill most of the water column from approximately 500 m depth down to the seabed (Figure 6), driving what we infer to be a full-ocean depth eastward flow at the north end of section D. However, this one station is insufficient to confirm whether this might be the southernmost core of steady eastward flow associated with the ACC or a transient feature associated with wind-forced variability or eddy activity.

[24] The temperature and salinity sections for each transect (Figure 6) all show CDW filling most of the offshore water column, hugging the continental slope, and shoaling toward the shelf edge. With the exception of stations 11 (Transect D) and 25 (Transect B), where the topmost 500 m have similar characteristics to the on-shelf CTD stations all the off-shelf stations have an UCDW subsurface potential temperature maximum between  $1.5$  and  $1.7^{\circ}\text{C}$  in the 300–00 m depth range. Beneath this lies LCDW characterized by a salinity maximum core ( $S > 34.72$  psu) which is typically found at around 700 m depth. Above the CDW and the thermocline, the upper ocean is composed of cold ( $\theta < 0^{\circ}\text{C}$ ) AASW (and WW) the upper portion of which appears continuous between the on-shelf and off-shelf regions. On all stations the WW signature begins at approximately 60 m deep, extending to approximately 100 m deep in the off-shelf region, but deepening over the shelf break to reach depths of 200–250 m at the on-shelf CTD stations.

[25] The water properties over the continental slope and shelf break suggest significant baroclinic structure in the currents associated with the sloping isopycnals surfaces, typically associated with salinity contours in cold waters such as these, but more closely related to the temperature contours in the nearly isohaline LCDW layer. On most sections, below the level of the shelf break, there is a general upward slope of the isopycnals toward the south, associated with the shoaling of the temperature maximum. Just above this between approximately 250 and 400 m depth, downward sloping isopycnals above the shelf edge are associated with the southward deepening of the WW layer and cooling of the UCDW temperature maximum core. The resulting horizontal density gradient is effectively a weak Antarctic Slope Front (ASF), a nearly circumpolar feature that is typically associated with the complete exclusion of CDW from the continental shelves [Whitworth *et al.*, 2008].

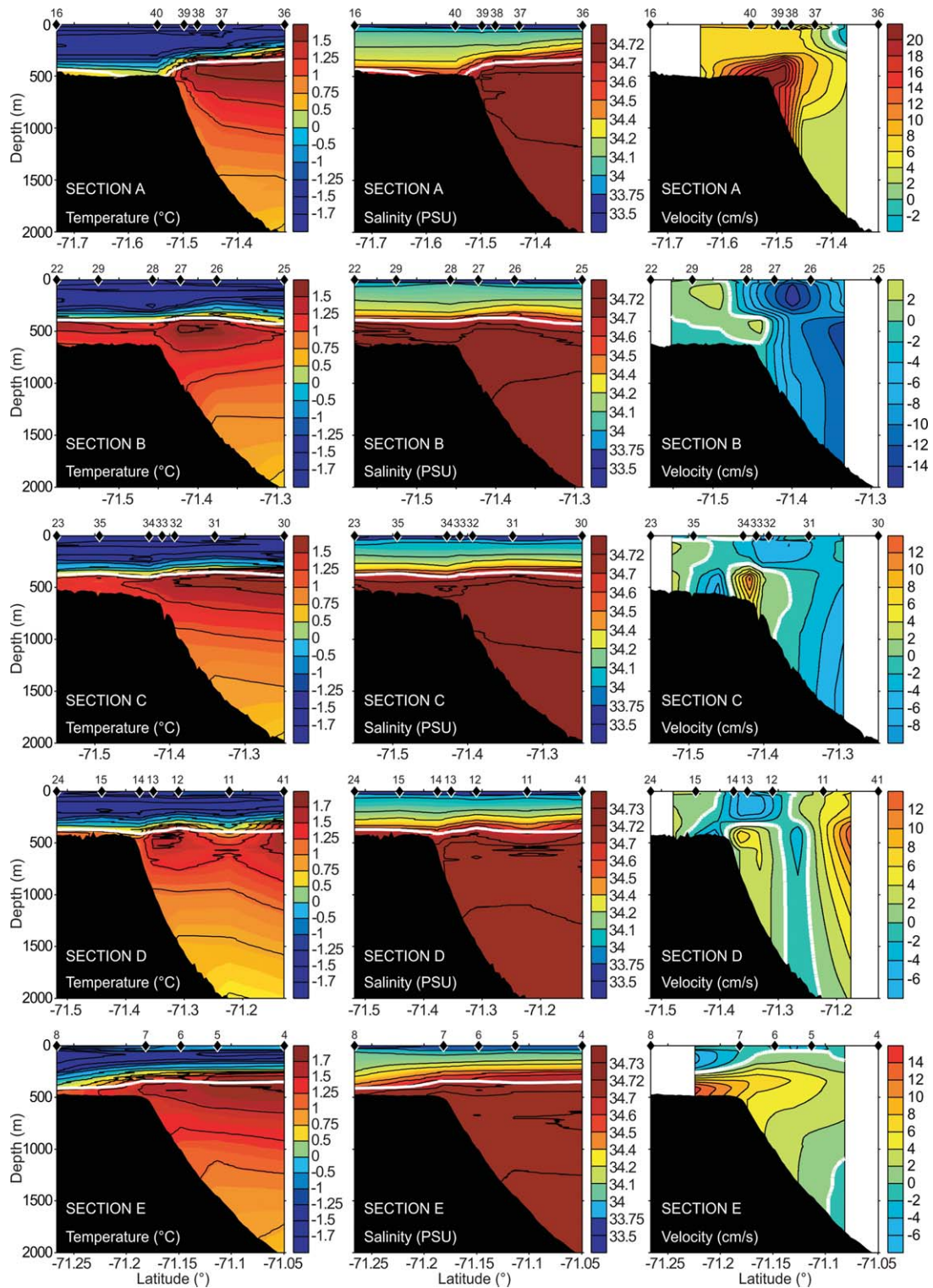


**Figure 6.** Potential temperature, salinity, and geostrophic velocity sections for each across-shelf transect (sections A–E). Numbered diamonds on the upper axes show the CTD locations. The white contour on the temperature and salinity sections is the  $\gamma^n = 28.00 \text{ kg m}^{-3}$  neutral density surface. The white contour on the velocity sections denotes the zero velocity line. Positive values are eastward flowing currents.

The ASF is found directly above the shelf edge, except in section E, which is the only transect located a significant distance from the trough (150 km to the east), where the gradient occurs a few kilometres onto the shelf.

[26] At the southern, on-shelf end of each section the neutral density line ( $\gamma^n = 28.00 \text{ kg m}^{-3}$ ) representing the upper boundary of the regional CDW [Whitworth *et al.*, 1998] is consistently found at 400 m ( $\pm 20$  m) depth.

However, the cooling of the CDW core beneath this contour depends on whether a section lies within the trough or not. Sections A, D, and E lie outside of the trough and include the five shallowest CTD stations in the entire data set. These five CTD stations are shown as blue lines in the  $\theta$ - $S$  plot (Figure 5) and were measured in water depths between 420 and 520 m. All of these stations are unique in that they lack the middepth temperature maximum found elsewhere at least 100 m above the seafloor overlying a layer of LCDW. Instead, the maximum temperatures, which range from 0.5 to 1°C, are found at the deepest point measured, a few meters from the seabed. CTD 40 is the most extreme example of this. Although the temperature just 2 m above the seabed is 0.72°C, only 6 m higher in the water column the temperature drops to 0.25°C and has  $\theta$ - $S$  properties of seawater found in the thermocline, as can be seen clearly in the temperature section (Figure 6—section A).

[27] In contrast, the on-shelf CTDs measured in the trough (stations 17–23) each have a pronounced middepth temperature maximum core with temperatures of up to 1.43°C, only 0.3°C cooler than those found in the off-shelf stations. Properties found within the trough are exemplified by CTD 22, highlighted by the green line in Figure 5. The temperature maximum there is found at 450 to 500 m depth, whereas the LCDW beneath has salinities greater than 34.72 psu, identical to the offshore LCDW source. The trough reaches 620 m depth, level with the off-shelf transition between LCDW and UCDW, so it is perhaps unsurprising that LCDW is found in the trough.

[28] Overall, the on-shelf CDW appears to derive from a mixture of offshore LCDW and UCDW, rather than from vertical and/or horizontal mixing between UCDW and AASW at the shelf break. If the on-shelf CDW were a mixture of offshore UCDW and on-shelf AASW, we would expect it to freshen and cool and follow a line in  $\theta$ - $S$  space between CDW and WW. Furthermore, even outside of the trough the  $\theta$ - $S$  properties found near the seafloor tend toward those of off-shelf LCDW (Figure 5).

[29] Most of the  $\theta$ - $S$  profiles across the ASF contained sharp short inversions within the thermocline suggesting complex mixing processes. An example of these inversions can be seen in CTD 22 (green line in Figure 5) with two steps found in the thermocline, one close to the WW core and the other one halfway between WW and CDW.

### 3.2. Geostrophic Velocity Sections

[30] The geostrophic velocity sections shown in Figure 6 are those obtained using the on-station pair-averaged SADC data that were detided using the empirically derived tide. Note that section D is longer than the others due to the addition of CTD station 41, which extended the section 6 km further north. In all of the velocity sections, the water column between the outermost pair of CTD stations (excluding CTD 41 in section D) located on the 2000 and 1500 m isobaths, experiences some westward flow (negative velocities), the strength, and spatial coverage of which varies between sections. Additionally, all sections show a surface-intensified core of westward flow in the topmost 300 m, beneath which the shear associated with the weak ASF generates an eastward undercurrent (positive velocities) that typically hugs the upper continental slope

and the outer portion of the shelf edge. The strength and extent of the undercurrent vary considerably between sections.

[31] Section A is situated just west of the trough and is dominated by the eastward flowing undercurrent, which is bottom intensified at the outer shelf edge (peak velocities in excess of 20 cm s<sup>-1</sup>) and continues down the continental slope, gradually weakening until the 1200 m isobath. At the offshore end of the section, a weak surface westward flow ( $\sim$ 4 cm s<sup>-1</sup>) exists in the upper 200 m. Section B is located further to the east, approximately halfway between the centreline and the eastern edge of the trough. Although there is some weak eastward flow at the on-shelf end of the section, the pronounced eastward undercurrent has all but disappeared over the slope. The entire water column offshore of the shelf edge flows westward at about 10 cm s<sup>-1</sup>, with some surface intensification in the upper 300 m reaching speeds of up to 20 cm s<sup>-1</sup>. Section C crosses the shelf break just inside the sidewall of the trough on its easternmost flank. Here, we see the reemergence of an eastward undercurrent located at the top of the shelf break as a clearly defined but considerably weaker core, both in size and strength compared with its upstream counterpart. Again, the water column above the slope has a surface-intensified westward flow that is nevertheless weaker than in section B. Section D is approximately 9 km further east, outside of the trough, and has similar properties to section C except that the core of undercurrent has shifted a little offshore. Again it has relatively low speeds compared with those seen on the westernmost, upstream section (section A). There is also a weak ( $\sim$ 4 cm s<sup>-1</sup>) westward flow above the lower portion of the slope with a slightly enhanced surface core ( $>$ 6 cm s<sup>-1</sup>) in the upper 400 m above the undercurrent. The northward extension of the section (station 41) picks up a full ocean depth eastward current reminiscent, possibly, though not conclusively, associated with the southernmost part of the ACC. This current has peak velocities of over 12 cm s<sup>-1</sup> at a depth of 400 m and an average of around 6 cm s<sup>-1</sup> over the entire water column. Finally, section E, which is located 150 km further to the east, is similar to section A. The undercurrent dominates the outer edge of the shelf and most of the upper continental slope down to 1500 m with the seabed-intensified core moving in excess of 10 cm s<sup>-1</sup>. Again, we see a surface intensified westward current directly above the undercurrent in the upper 300 m with speeds of 10 cm s<sup>-1</sup>. The main difference between sections A and E is that in the latter the undercurrent and the ASF extend further onto the shelf.

## 4. Discussion

[32] On-shelf flow of CDW within the trough was reported previously by Walker *et al.* [2007], from an analysis of the data from section Tr. Our more complete analysis of the entire JR84 data set presented above shows that there are two ways by which the trough can promote on-shelf flow: the deeper topography relative to the off-shelf thermocline and the interaction of the topography with the shelf edge currents, especially the eastward undercurrent associated with the ASF.

[33] Where the trough is present (sections B and C), the extra depth of the seabed clearly permits a significantly

greater volume of water beneath the  $\gamma^n = 28.00 \text{ kg m}^{-3}$  contour on-shelf, as stated earlier by Walker *et al.* [2007]. Furthermore, core CDW temperatures within the trough are higher than elsewhere in our study region, and only the waters within the trough are warm enough to be regarded as source waters for the deep trough in Pine Island Bay [Jacobs *et al.*, 2011]. Similar findings have been reported for seabed troughs located to the east around  $103^\circ\text{W}$  [Jacobs *et al.*, 2011] and to the west around  $119^\circ\text{W}$  [Wahlin *et al.*, 2010]. Of these the eastern trough connects with Pine Island and Thwaites glaciers, while the western trough leads to Dotson Ice Shelf and the eastern end of Getz Ice Shelf. The sill of the western trough is somewhat shallower [Nitsche *et al.*, 2007] so that the layer of CDW flowing on-shelf is correspondingly thinner and cooler [Wahlin *et al.*, 2010]. In the east, the depth of the trough is similar, but the main thermocline is shallower [Jacobs *et al.*, 2011] so a thicker and warmer layer of CDW may access the shelf there [Jacobs *et al.*, 2012]. Schodlok *et al.* [2012] argue that the eastern trough is the main source of heat for PIG, implying only a minor role for the central trough. However, once on shelf, water from the central trough flows to the east to merge with the eastern inflow [Thoma *et al.*, 2008; Schodlok *et al.*, 2012] and based on analysis of data collected in the summer of 2012, Nakayama *et al.* [2013] argue that the central trough supplies about two thirds of the CDW in the mixture that eventually fills the Pine Island trough. Although the eastern trough does appear to supply warmer CDW, thermocline depth over the inner shelf may play a stronger role than CDW core temperature in setting glacial melt rates [Jacobs *et al.*, 2011]. The relative roles of the two CDW sources, and that of local surface forcing over the shelf, in setting the thermocline depth remain unclear.

[34] Although the seabed depth within the trough allows a greater thickness of CDW on shelf, the eastward undercurrent appears to be what actually carries off-shelf CDW into the trough. The undercurrent is situated in the water column such that it carries source CDW along the shelf edge and upper slope and our data suggest that it turns on-shelf when it encounters the trough (Figure 6). The dramatic change in the strength of the undercurrent between section A, just upstream of the trough, and section B, toward its downstream edge, implies that most of the flow was deflected on-shelf when it encountered the southward turn of the isobaths at the upstream edge of the trough. Section C, on the downstream flank of the trough, shows the eastward flow reestablishing itself, possibly as a result of CDW recirculating out of the trough, whereas downstream of the trough at section D the undercurrent has been deflected back onto the upper slope by the northward turn of the isobaths. The much weaker undercurrent downstream of the trough compared with upstream suggests a significant net on-shelf flow within the trough. At section E, some 150 km further along the shelf edge, the undercurrent is again a major feature over the upper slope and shelf edge, similar in extent although still weaker than seen in section A. The main difference between sections A and E is that in the latter the eastward flow is stronger on the outer shelf than over the slope.

[35] The conclusion that the undercurrent turns onto the shelf is supported by the data collected across the trough

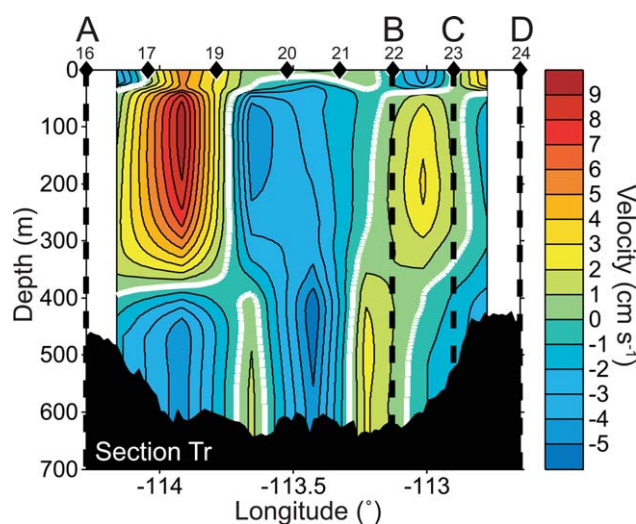


**Figure 7.** Velocity section across the trough (section Tr). Negative values represent on-shelf poleward flow and the white line is the zero velocity contour. CTD station positions and labels are marked at the top with black diamonds. The labeled thick dashed black lines show where the across-shelf sections A–D perpendicularly bisect this section.

approximately 20–25 km inshore of the shelf edge (section Tr). Figure 7 shows the geostrophic velocity section derived from these data (CTDs 16–24). Over the central and western parts of the trough, beneath 400m, there are two main cores of inflow (blue, negative values) divided by a weak counter flow between CTDs 19 and 20. Sections A and B intersect section Tr either side of this inflow, so the dramatic weakening of the undercurrent between these two sections is consistent with it feeding the southward flow. Additionally, there is a relatively weak offshore flowing core between stations 21 and 23, possibly a recirculation of part of the inflow back out of the trough on its downstream side feeding the renewed undercurrent seen in sections C and D. It is also apparent in Figure 7 that the strongest off-shelf (northward) flow here is in the upper water column between the surface and 400 m deep between CTDs 16 and 19. Although an interesting feature, we are mainly concerned in this study with the deeper flow of CDW.

[36] CTD stations 11 and 25 that were both located in 2000 m water depth at the base of the continental rise differ from all of the other off-shelf stations. The upper 500 m of the water column at these two locations has water properties identical to the on-shelf water column, with a thicker layer of AASW above the  $\gamma^n = 28.00 \text{ kg m}^{-3}$  density contour. This may indicate eddy activity either associated with instability of the ASF or with the dynamics of the undercurrent and its interaction with the trough, particularly where the isobaths make a sharp turn onshore and offshore.

[37] Previously unreported in observations of this area, the eastward undercurrent and its apparent role in the on-shelf transport of CDW provide new insight that is of value in reassessing earlier results from a coarse-resolution regional ice-ocean model of the Amundsen Sea [Thoma *et al.*, 2008]. Two key findings of that study, namely a clear correlation between inner shelf thermocline depth and on-

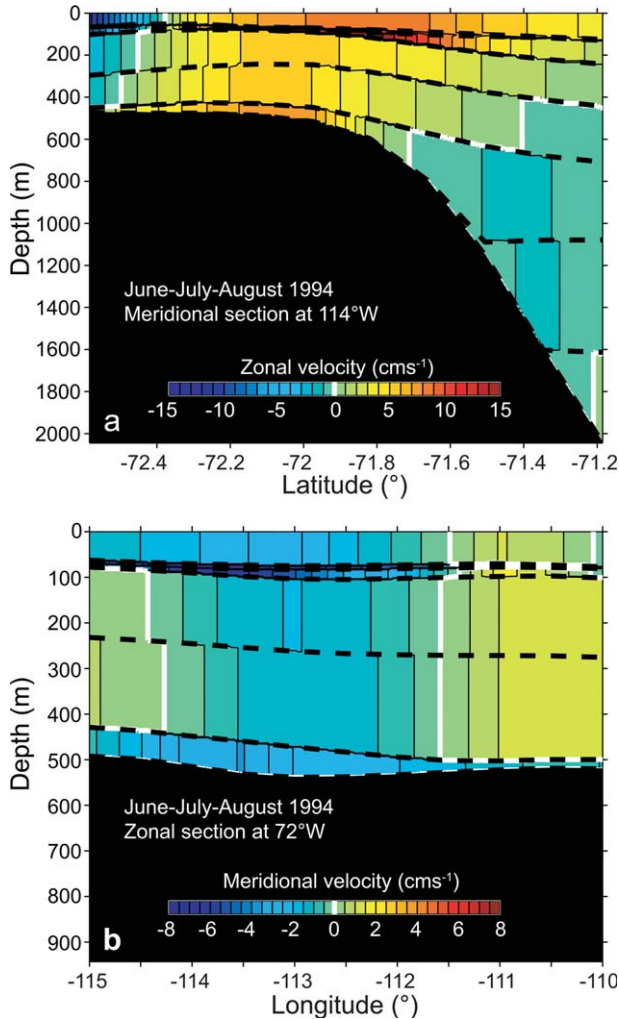


**Figure 8.** (a) Across-shelf section taken from a regional model of the Amundsen Sea at 114°W [Thoma *et al.*, 2008]. Positive values represent eastward along-shelf flow. Data represent the mean flow from the model for the three winter months of 1994. (b) Along-shelf (trough) section at 72°S showing the meridional velocity taken from the same model. Negative values are southward along-trough flow.

shelf flow of CDW through the central trough and a weaker but still significant correlation between onshelf CDW flow and local wind forcing, have recently been drawn into question [Schodlok *et al.*, 2012; Arneborg *et al.*, 2012]. The model was based on the Miami Isopycnic Coordinate Ocean Model [Bleck *et al.*, 1992] was run on a coarse-resolution (17 km at the shelf edge) grid with smoothed bathymetry and was forced with surface temperature and pressure NCEP reanalysis data [Kalnay *et al.*, 1996]. Figure 8 shows two velocity sections extracted from the model results at the approximate locations of our sections A and Tr. Note that smoothing of the model bathymetry produces a continental slope that is broader and less steep than the true bathymetry and an on-shelf trough that is little more than a slight dip in the seabed between 112°W and 114°W. In the across-shelf, zonal velocity section (Figure 8a), the model shows a bottom-intensified eastward undercurrent on the apex of the continental slope, while the across-

trough, meridional velocity section (Figure 8b) shows a bottom-intensified southward flow within the dip beneath 400 m. Although other features of these sections do not match well with the observations, these bottom-intensified features are at least qualitatively similar to the undercurrents we have observed, remarkably so given the coarseness of the model grid and the smoothness of the model bathymetry. In the model, the variability in the strength and thickness of the eastward undercurrent was the main process responsible for driving variability in the flow of CDW onto the shelf [Thoma *et al.*, 2008]. Thus, our observations of the undercurrent provide support for these findings of the model, whereas the model results support the inference that the observed undercurrent is a key process in moving CDW onshore.

[38] Other than the presence of an undercurrent, there are large differences between the observations and the model results. The main origin of the differences is that the modeled front above the continental shelf edge, indicated by the shoreward deepening of the isopycnal layer interfaces, and the associated current shear are very weak features compared with the observations. This is a product both of the coarse model resolution and the fact that it was run within a closed domain, resulting in a weak ACC and a general relaxation of all the associated fronts. As a result, the modeled eastward undercurrent is weak or nonexistent in summer when the surface flow is driven to the west by a predominantly easterly wind stress, but appears and strengthens during winter when the wind forcing is predominantly westerly and drives a full-depth, bottom-intensified eastward flow. Thus, the seasonality of the inflow modeled by Thoma *et al.* [2008] will have been exaggerated by a lack of frontal baroclinicity leading to shutdown of the inflow in the summer months. Our late summer observations suggest that with stronger baroclinicity at the shelf edge in reality the undercurrent is likely to be a year-round feature, although seasonal changes in its strength could still be driven by changes in wind stress acting on the barotropic flow over the shelf edge.

[39] Arneborg *et al.* [2012] analyzed current meter data from a neighboring trough in the Amundsen Sea that channels CDW toward the Dotson and Getz ice shelves. Their observations of a persistent baroclinic flow within the trough are consistent with our picture of such flows being supplied from the shelf edge by an undercurrent associated with the persistent ASF. However, they find no correlation between wind forcing and on-shelf transport of CDW, contradicting the results of Thoma *et al.* [2008]. It remains unclear whether this discrepancy is a result of geographical or temporal differences, the shortness of the observational record or an indication that our interpretation of the model is flawed. Although the model setup undoubtedly suppressed other sources of variability, such as instability in the ACC and its associated fronts, which will be present in the observations, the response to the wind forcing was a robust feature that remained qualitatively unaltered in numerous sensitivity studies. Although that response may have been exaggerated by a lack of baroclinicity in the ASF, even a much weaker response in the inner shelf thermocline depth could have a major impact on the melt rate of the Amundsen Sea ice shelves [Jacobs *et al.*, 2011].

[40] An Antarctic slope undercurrent has been observed at about 1000 m depth on the continental slope in the eastern Weddell Sea [Heywood *et al.*, 1998; Chavanne *et al.*, 2010], associated with the much stronger and deeper reaching ASF found in that region. Although the strong front gives a strongly sheared current, the persistent easterly wind stress gives a much stronger surface flow to the west and a correspondingly weaker undercurrent. Chavanne *et al.* [2010] reported changes in the strength and depth of the undercurrent caused by shifts in the barotropic component of the flow that they attributed to the passage of coastally trapped waves.

[41] Klinck [1996] used a numerical model to examine the behavior of along-shelf flows when they encountered an idealized trough finding that the flow would either turn onto the shelf within the canyon, or off the shelf, depending on the direction of the along-shelf current. For the northern (southern) hemisphere, a left- (right-) bounded flow would drive upwelling within the trough and strong exchange between the ocean and shelf. Analogous to our observed undercurrent, the modeled along-shelf current turned shoreward as soon as it encountered the trough, and a greatly weakened along-shelf current appeared beyond the downstream edge of the trough. The upwelling suggested by these model results might help to explain the strong LCDW signature observed within the trough.

[42] Although the presence of CDW on the continental shelves of the Amundsen and Bellingshausen seas makes the two regions appear superficially similar, the key processes that drive on-shelf flow of CDW may be subtly different. Orsi *et al.* [1995] locate the southern boundary (SB) of the ACC and the SACCF considerably north of the shelf break at 115°W, with both coming close to the continental margin at around 100°W then hugging the continental slope into the Bellingshausen Sea. Our data are consistent with this, clearly showing the SACCF at the bottom of the continental slope, near the 3000 m isobath, at 101°W, but located to the north of our sections elsewhere. At the northern end of section D, we inferred a full-depth eastward current, whose properties lead us to speculate that it may be the SB of the ACC, but the evidence is equivocal, especially given that the northernmost CTD station was not occupied at the same time as the others on the section. Thus, we conclude that CDW inflows to the Amundsen Sea continental shelf are determined by the current structure and variability associated with the weak ASF. In this respect, they differ from analogous inflows in the eastern Bellingshausen Sea where there is no ASF, the SACCF hugs the continental slope, and the current structure and variability associated with the SACCF appear to drive the inflows [Klinck *et al.*, 2004; Moffat *et al.*, 2009].

[43] Whitworth *et al.* [1998] suggested that the ASF is absent in the eastern Amundsen Sea, being traceable from around 120°W westward toward the Ross Sea. However, most of the observational data in the Amundsen Sea have been collected since that study. All of our across-shelf sections show the signature of a weak slope front and an analogous feature was found by Jacobs *et al.* [2011] near 103°W. Further to the west in the Ross Sea, a distinctly stronger ASF exists [Jacobs, 1991], so the Amundsen Sea appears to be a transition zone between the Ross and the Bellingshausen seas, where the ASF weakens and the ACC moves close to the continental margin.

## 5. Summary

[44] We have analyzed oceanographic data from a region of the Amundsen Sea continental shelf break where a cross-shelf trough that extends from Pine Island Bay meets the shelf edge. Our observational data set includes five CTD/ADCP sections that cross the shelf edge and upper slope and a sixth that parallels the shelf edge a short distance on-shelf. We have presented the water mass and current structure observed along these sections. All of the across-shelf sections show the presence of CDW on the continental shelf. The CDW found outside of the trough is cooled to 1°C or less while maintaining densities very similar to the offshore source, while within the trough a considerably thicker layer of CDW is found, with temperatures up to 1.46°C and  $\theta$ - $S$  properties identical to offshore LCDW. These findings highlight the role of the trough in permitting on-shelf flow of CDW and in promoting upwelling that allows LCDW to contribute to the inflow.

[45] None of the shelf-break sections between 108°W and 115°W appear to cross the SACCF or the SB of the ACC, although there is evidence suggesting that the SB may be not far to the north. Further to the east, we find evidence that the SACCF meets the continental slope at approximately 101°W north of Thurston Island. All of the shelf break sections display marked baroclinic features associated with a weak ASF. At the surface, there is westward flow, beneath which pronounced shear within the water column drives an eastward slope undercurrent that appears at or near to the top of the slope. This undercurrent, which is entirely composed of CDW, turns onto the shelf when it encounters the shelf edge trough, transferring offshore CDW into the shelf regime, where it can ultimately drive melting of the Amundsen Sea ice shelves. As the undercurrent turns south onto the shelf, the along-shelf component dramatically weakens within the trough mouth. The on-shelf flow is captured in the (perpendicular) across-trough section which shows a broad inflow over the central part of the trough. Immediately downstream of the trough, the undercurrent remains weak suggesting that the bulk of it enters the trough with only a small portion recirculating back out along the shelf edge. Considerably further downstream the undercurrent is reestablished, and we assume that this stronger flow probably turns on-shelf when it encounters the next trough mouth at approximately 103°W.

[46] This behavior is captured in both idealized and realistic models, the latter suggesting that the amount of on-shelf CDW transport is directly related to the strength of the undercurrent. Variability in this modeled transport resulted from seasonal changes in the surface wind field either strengthening or weakening the undercurrent. Our observations show stronger shears over the slope that drive a stronger undercurrent than that in the model, suggesting that seasonal variability may be overestimated in the model, but without any time-series observations it is impossible to verify the behavior of the undercurrent on seasonal or longer timescales. If this undercurrent is a permanent feature, it could continuously supply CDW to the shelf, and if its strength is determined by components of the wind field that are influenced by far-field forcing [Stieg *et al.*, 2012], the processes described here may help to explain the observed increase in glacial melt rates in the Amundsen Sea Embayment.

[47] **Acknowledgments.** We wish to thank the officers and crew of the *RRS James Clark Ross* and also J. Dowdeswell and J. Evans for processing and supplying the acoustic multibeam data. This work was funded by the British Antarctic Survey and the Natural Environment Research Council's Autosub Under Ice Thematic Programme (award reference NER/T/S/2000/00987) and subsequent programme (award reference NE/G001367/1).

## References

- Allen, J. T. (1995), Subtidal and tidal currents in the vicinity of the Iceland-Faeroes front, *J. Atmos. Oceanic Technol.*, *12*(3), 567–588, doi:10.1175/1520-0426(1995)012<0567:SATCIT>2.0.CO;2.
- Arneborg, L., A. K. Wåhlin, G. Björk, B. Liljebladh, and A. H. Orsi (2012), Persistent inflow of warm water onto the central Amundsen shelf, *Nat. Geosci.*, *5*, 876–880, doi:10.1038/NCEO1644.
- Bamber, J. L., R. E. M. Riva, B. L. A. Vermeersen, and A. M. LeBrocq (2009), Reassessment of the potential sea-level rise from a collapse of the West Antarctic ice sheet, *Science*, *324*, 901–903, doi:10.1126/science.1169335.
- Bleck, R., C. Rooth, D. Hu, and L. T. Smith (1992), Salinity-driven thermocline transients in a wind- and thermohaline-forced isopycnic coordinate model of the North Atlantic, *J. Phys. Oceanogr.*, *22*(12), 1486–1505, doi:10.1175/1520-0485(1992)022<1486:SDTTIA>2.0.CO;2.
- Candela, J., R. C. Beardsley, and R. Limeburner (1992), Separation of tidal and subtidal currents in ship-mounted acoustic Doppler current profiler observations, *J. Geophys. Res.*, *97*(C1), 769–788, doi:10.1029/91JC02569.
- Chavanne, C. P., K. J. Heywood, K. W. Nicholls, and I. Fer (2010), Observations of the Antarctic Slope Undercurrent in the southeastern Weddell Sea, *Geophys. Res. Lett.*, *37*, L13601, doi:10.1029/2010GL043603.
- Ding, Q., E. J. Steig, D. S. Battisti, and M. Kuttel (2011), Winter warming in West Antarctica caused by central Pacific warming, *Nat. Geosci.*, *4*, 398–403, doi:10.1038/ngeo1129.
- Heywood, K. J., R. A. Locarnini, R. D. Frew, P. F. Dennis, and B. A. King (1998), Transport and water masses of the Antarctic Slope Front system in the eastern Weddell Sea, in *Ocean, Ice and Atmosphere: Interactions at the Antarctic Continental Margin*, *Antarctic Res. Ser.*, vol. 75, edited by S. S. Jacobs and R. F. Weiss, pp. 203–214, AGU, Washington, D. C., doi:10.1029/AR075p0203.
- Jackett, D. R., and T. J. McDougall (1997), A neutral density variable for the world's oceans, *J. Phys. Oceanogr.*, *27*(2), 237–263, doi:10.1175/1520-0485(1997)027<0237:ANDVFT>2.0.CO;2.
- Jacobs, S. S., (1991), On the nature and significance of the Antarctic Slope Front, *Mar. Chem.*, *35*, 9–24, doi:10.1016/S0304-4203(09)90005-6.
- Jacobs, S. S., H. H. Hellmer, and A. Jenkins (1996), Antarctic ice sheet melting in the southeast Pacific, *Geophys. Res. Lett.*, *23*(9), 957–960, doi:10.1029/96GL00723.
- Jacobs, S. S., A. Jenkins, C. F. Giulivi, and P. Dutrieux (2011), Stronger ocean circulation and increased melting under Pine Island Glacier ice shelf, *Nat. Geosci.*, *4*, 519–523, doi:10.1038/NCEO1188.
- Jacobs, S. S., A. Jenkins, H. Hellmer, C. Giulivi, F. Nitsche, B. Huber, and R. Guerrero (2012), The Amundsen Sea and the Antarctic Ice Sheet, *Oceanography*, *25*, 154–163, doi:10.5670/OCEANOGRAPHY.2012.90.
- Jenkins, A., P. Dutrieux, S. S. Jacobs, S. D. McPhail, J. R. Perrett, A. T. Webb, and D. White (2010), Observations beneath Pine Island Glacier in West Antarctica and implications for its retreat, *Nat. Geosci.*, *3*, 468–472, doi:10.1038/NCEO890.
- Joughin, I., B. E. Smith, and D. M. Holland (2010), Sensitivity of 21st century sea level to ocean-induced thinning of Pine Island Glacier, Antarctica, *Geophys. Res. Lett.*, *37*, L20502, doi:10.1029/2010GL044819.
- Kalnay, E., et al. (1996), The NCEP/NCAR 40-year reanalysis project, *Bull. Am. Meteorol. Soc.*, *77*(3), 437–471, doi:10.1175/1520-0477(1996)077<0437:TNYRP>2.0.CO;2.
- King, B. A., and E. B. Cooper (1994), GPS & DGPS: Navigation tools for shipboard ADCPs, *Sea Technol.*, *35*(3), 10–15.
- Klinck, J. M. (1996), Circulation near submarine canyons: A modeling study, *J. Geophys. Res.*, *101*(C1), 1211–1223, doi:10.1029/95JC02901.
- Klinck, J. M., E. E. Hofmann, R. C. Beardsley, B. Salihoglu, and S. Howard (2004), Water-mass properties and circulation on the west Antarctic peninsula continental shelf in austral fall and winter 2001, *Deep Sea Res. II*, *51*, 1925–1946, doi:10.1016/j.dsr2.2004.08.001.
- Moffat, C., B. Owens, and R. C. Beardsley (2009), On the characteristics of Circumpolar Deep Water intrusions to the west Antarctic Peninsula Continental Shelf, *J. Geophys. Res.*, *114*, C05017, doi:10.1029/2008JC004955.
- Nakayama, Y., M. Schroeder, and H. H. Hellmer (2013), From circumpolar deep water to the glacial meltwater plume on the Amundsen Shelf, *Deep-Sea Res.*, *77*, 50–62.
- Nitsche, F. O., S. S. Jacobs, R. D. Larter, and K. Gohl (2007), Bathymetry of the Amundsen Sea continental shelf: Implications for geology, oceanography, and glaciology, *Geochem. Geophys. Geosyst.*, *8*, Q10009, doi:10.1029/2007GC001694.
- Orsi, A. H., T. Whitworth III, and W. D. Nowlin, Jr. (1995), On the meridional extent and fronts of the Antarctic Circumpolar Current, *Deep Sea Res.*, Part I, *42*(5), 641–673, doi:10.1016/0967-0637(95)00021-W.
- Padman, L., H. A. Fricker, R. Coleman, S. Howard, and S. Erofeeva (2002), A new tidal model for the Antarctic ice shelves and seas, *Ann. Glaciol.*, *34*, 247–254, doi:10.3189/172756402781817752.
- Rignot, E. (2002), Ice-shelf changes in Pine Island Bay, Antarctica, 1947–2000, *J. Glaciol.*, *48*(161), 247–256, doi:10.3189/172756502781831386.
- Rignot, E. (2008), Changes in West Antarctic ice stream dynamics observed with ALOS PALSAR data, *Geophys. Res. Lett.*, *35*, L12505, doi:10.1029/2008GL033365.
- Rignot, E., J. L. Bamber, M. R. van den Broeke, C. Davis, Y. Li, W. J. van de Berg, and E. van Meijgaard (2008), Recent Antarctic ice mass loss from radar interferometry and regional climate modelling, *Nat. Geosci.*, *1*, 106–110, doi:10.1038/ngeo102.
- Schodlok, M. P., D. Menemenlis, E. Rignot, and M. Studinger (2012), Sensitivity of the ice-shelf/ocean system to the sub-ice-shelf cavity shape measured by NASA IceBridge in Pine Island Glacier, West Antarctica, *Ann. Glaciol.*, *53*, doi:10.3189/2012AoG60A073.
- Schoof, C. (2007), Ice sheet grounding line dynamics: Steady states, stability, and hysteresis, *J. Geophys. Res.*, *112*, F03S28, doi:10.1029/2006JF000664.
- Shepherd, A., D. J. Wingham, J. A. D. Mansley, and H. F. J. Corr (2001), Inland thinning of Pine Island Glacier, West Antarctica, *Science*, *291*, 862–864, doi:10.1126/science.291.5505.862.
- Shepherd, A., D. J. Wingham, and E. Rignot (2004), Warm ocean is eroding West Antarctic ice sheet, *Geophys. Res. Lett.*, *31*, L23402, doi:10.1029/2004GL021106.
- Steig, E. J., Q. Ding, D. S. Battisti, and A. Jenkins (2012), Tropical forcing of Circumpolar Deep Water inflow and outlet glacier thinning in the Amundsen Sea Embayment, West Antarctica, *Ann. Glaciol.*, *53*, 19–28, doi:10.3189/2012AoG60A110.
- Thoma, M., A. Jenkins, D. Holland, and S. Jacobs (2008), Modelling Circumpolar Deep Water intrusions on the Amundsen Sea continental shelf, Antarctica, *Geophys. Res. Lett.*, *35*, L18602, doi:10.1029/2008GL034939.
- Thorpe, S. E., K. J. Heywood, M. A. Brandon, and D. P. Stevens (2002), Variability of the southern Antarctic Circumpolar Current front north of South Georgia, *J. Mar. Syst.*, *37*, 87–105, doi:10.1016/S0924-7963(02)00197-5.
- Timmermann, R., et al. (2010), A consistent data set of Antarctic ice sheet topography, cavity geometry, and global bathymetry, *Earth Syst. Sci. Data*, *2*, 261–273, doi:10.5194/essd-2-261-2010.
- Wåhlin, A. K., X. Yuan, G. Björk, and C. Nohr (2010), Inflow of warm Circumpolar Deep Water in the central Amundsen shelf, *J. Phys. Oceanogr.*, *40*, 1427–1434, doi:10.1175/2010JPO4431.1.
- Walker, D. P., M. A. Brandon, A. Jenkins, J. T. Allen, J. A. Dowdeswell, and J. Evans (2007), Oceanic heat transport onto the Amundsen Sea shelf through a submarine glacial trough, *Geophys. Res. Lett.*, *34*, L02602, doi:10.1029/2006GL028154.
- Whitworth, T., III, A. H. Orsi, S.-J. Kim, and W. D. Nowlin Jr. (1998), Water masses and mixing near the Antarctic Slope Front, in *Ocean, Ice and Atmosphere: Interactions at the Antarctic Continental Margin*, *Antarctic Res. Ser.*, vol. 75, edited by S. S. Jacobs and R. F. Weiss, pp. 1–27, AGU, Washington, D. C., doi:10.1029/AR075p0001.
- Wingham, D. J., A. Ridout, R. Scharroo, R. Arthern, and C. K. Shum (1998), Antarctic elevation change from 1992 to 1996, *Science*, *282*, 456–458, doi:10.1126/science.282.5388.456.